Disorder-induced incoherent scattering losses in photonic crystal waveguides: Bloch mode reshaping, multiple scattering, and breakdown of the Beer-Lambert law

M. Patterson and S. Hughes[*]
Department of Physics, Queen's University, Kingston, Ontario, Canada K7L 3N6

S. Schulz, D. M. Beggs, T. P. White, L. O'Faolain, and T. F. Krauss[†]
School of Physics and Astronomy, University of St. Andrews, Fife KY16 9SS, United Kingdom
(Received 24 July 2009; revised manuscript received 14 September 2009; published 5 November 2009)

Through a combined theoretical and experimental study of disorder-induced incoherent scattering losses in slow-light photonic crystal slab waveguides, we show the importance of Bloch mode reshaping and multiple scattering. We describe a convenient and fully three-dimensional theoretical treatment of disorder-induced extrinsic scattering, including the calculation of backscatter and out-of-plane losses per unit cell, and the extrapolation of the unit-cell loss to the loss for an entire disordered waveguide. The theoretical predictions, which are also compared with recent measurements on dispersion engineered silicon waveguides, demonstrate the failure of the Beer-Lambert law due to multiple scattering. We also explain why the previously assumed group velocity scalings of disorder-induced loss break down in general.

I. INTRODUCTION

Photonic crystal (PC) waveguides are an emerging class of nanoengineered optical structure in which light may propagate at speeds much slower than the vacuum speed of light,[1,2] leading to enhanced linear and nonlinear optical effects,[3] and to the delay and storage of light.[4] Although these waveguides are usually, by design, intrinsically lossless, slow-light propagation amplifies extrinsic scattering from minute fabrication imperfections leading to large propagation losses.[5–8] Indeed, the role of scattering losses in nanophotonic structures such as PC waveguides is now regarded as one of the most important issues preventing the exploitation of practical nanoscale optical devices. The physics of disorder-induced scattering is also of significant fundamental interest, and can frequently lead to interesting behavior such as Anderson localization[9,10] and random lasing.[11]

Recently, there has been significant interest in developing intuitive scaling relations for PC waveguides that relate the scattering losses to the group velocity.[6–8] A common model is that the out-of-plane and backscatter losses scale inversely with group velocity (v_g) and group-velocity squared, respectively. These optical losses are analyzed typically using the famous Beer-Lambert law, where the intensity decays exponentially with distance. These scaling rules make physical sense, since as the light slows down, the local photon density of states increases inversely with the group velocity; what looks like a 1 nm bump at $v_g = c$, where c is the speed of light in vacuum, may look like 10 nm at $v_g = c/10$ as the effective optical length increases. While these generally well accepted scaling rules are valuable for building intuition about how device designs will perform, they neglect two essential ingredients: (i) the role of multiple scattering, which is neglected through use of the Beer-Lambert law, and which has been demonstrated directly in the regime of coherent scattering,[12] and (ii) the contribution of the Bloch mode electric field distribution to the loss. The need to account for multiple scattering has been predicted for two-dimensional (2D) PC structures, and implied for three-dimensional (3D) structures, by Ref. 13; and experimentally observed by Ref. 14. To our knowledge, no one has yet presented either calculations or experiments for directly showing the breakdown of the Beer-Lambert law due to multiple scattering for the ensemble average transmission loss (where the ensemble average is obtained by averaging the transmission spectra over many nominally identical experimental samples) for 3D planar PCs, where it is not clear if the law is valid.

In this work, we study disorder-induced propagation losses in planar PC waveguides to show, both theoretically and experimentally, that the Beer-Lambert law breaks down, even for very low degrees of fabrication disorder. This disagreement is particularly significant in the slow-light regime where multiple scattering[12–14] must to be taken into account and leads to losses that are, surprisingly, lower than those predicted from the Beer-Lambert law. From a theoretical perspective, we extend previous, fully 3D, treatments of incoherent scattering[6] to include multiple-scattering events, and we self-consistently account for changes in the Bloch mode reshaping as a function of frequency. We subsequently demonstrate the breakdown of the Beer-Lambert law for a planar PC waveguide and provide a rigorous but straightforward method for computing ensemble average scattering losses between waveguides of different lengths. We obtain good agreement between theory and transmission loss measurements on state-of-the-art dispersion-engineered silicon waveguides, and highlight that previously assumed scaling of loss as a function of group velocity must be revised on a number of fronts. These results are both surprising and important in their implications, as they suggest that present analysis techniques of PC waveguide measurements will not work if the Beer-Lambert law is employed; moreover, they suggest that multiple scattering actually helps to reduce the overall transmission losses, which is highly unusual, if not unique, for a 3D waveguide system.
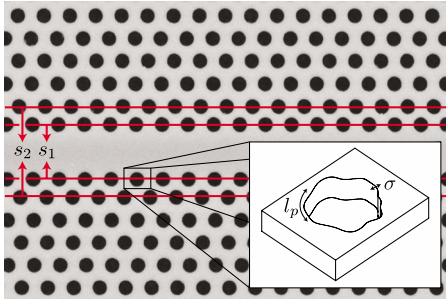
FIG. 1. (Color online) A SEM image of a typical dispersion engineered W1 with the first and second row offsets s_1 and s_2 schematically illustrated. Inset: schematic of a hole with disordered perimeter and straight side walls. We describe the statistical properties of the disorder with a RMS roughness σ and a correlation length l_p measured around the circumference.

II. DESIGN, FABRICATION, AND GROUP INDEX CALIBRATION

PC waveguides with tailored dispersion properties[15–18] are best suited for slow-light studies, as their group velocity can be adjusted (engineered) over a large spectral range. Our preferred tailoring method is to begin with a planar W1 waveguide formed, e.g., by omitting a row of holes in a triangular PC lattice. We then laterally shift the first and second rows of holes adjacent to the defect by a distances s_1 and s_2, respectively (refer to Fig. 1). This alters the nature of the PC waveguide, thus changing the position of the band-gap-guided mode relative to the index guided mode.[19] As these two modes anticross, the local shape of the dispersion curve is altered. This is a particularly powerful technique as the hole position may be controlled with very high precision (~ 1 nm) and also provides a wider operating range relative to other approaches.[15] Consequently, we are able to create a region of low-dispersion slow light with a range of specified values and with an optimized bandwidth.

The devices were fabricated on a SOITEC silicon-on-insulator wafer, consisting of a 220-nm-thick silicon guiding layer on a 2000-nm-thick silica buffer layer. The PC pattern was defined in ZEP-520A electron beam resist using a VISTEC VB6 electron beam writer with a 1.2 mm write field operating at 100 keV, thereby minimizing the effects of stitching errors on the PC waveguides. The pattern was transferred into the silicon layer using reactive ion etching with a combination of SF_6 and CHF_3 gases. Photolithographically defined windows were then opened in the photoresist above the photonic crystal regions and the air bridge created using a hydrofluoric acid wet etch. The fabrication process is very similar to that of Refs. 17 and 20. Coupling regions, as described in Refs. 17 and 21 were used to aid coupling of light in the slow-light regime. An example of the fabricated waveguide is shown in Fig. 1.

We fabricated a number of $s_1 = -48$ nm, $s_2 = 16$ nm, periodicity $a = 410 \pm 1$ nm, and radius $r = 0.286a = 118 \pm 10$ nm, 220 ± 10 nm thick membrane waveguides with different lengths. As discussed in Ref. 22, there can be a large systematic error in the radius and slab thickness when fabricating these devices. The experimental group index is measured
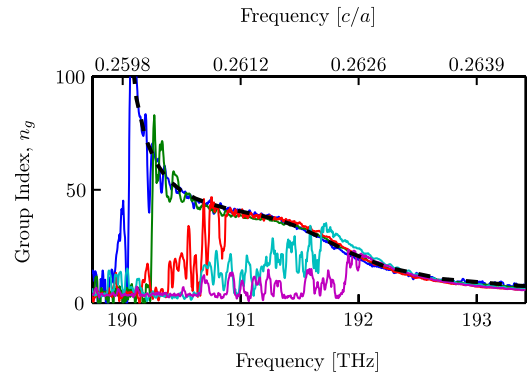

FIG. 2. (Color online) Measured group index for three different sample lengths (in order of decreasing maximum resolvable group index): 180 μm (blue), 300 μm (green), 700 μm (red), 900 μm (cyan), and 1500 μm (magenta). The fitted group index ($r = 112$ nm) is shown with the dashed black curve. The slow-light measurement is limited by the resolution of the optical spectrometer, which limits the maximum group delay that can be measured from interference fringes. It is this, rather than low transmission, which causes the apparent group indices to deviate so dramatically from the fit below a certain frequency, depending on the sample length. In the theory fit, a systematic frequency shift of 2.7 THz, has been applied to account for uncertainty in the slab thickness.

using Fourier-transform spectral interferometry[23] and shown in Fig. 2 for waveguides of different length. We model the properties of the ideal waveguides (no disorder) with a frequency-domain plane-wave expansion technique, using a freely available software package,[24] though any mode solving techniques can be used. Assuming no significant changes in the band structure due to disorder, we then slightly adjusted the estimated radius of the holes by around 6 nm to obtain reasonable fits to the experimental group index. A smaller radius of $0.274a = 112$ nm (dashed black) was found to better fit the observed dispersion, and we use this value in the following calculations.

III. THEORY OF DISORDER-INDUCED SCATTERING

Previously, several groups[6–8] reported various extrinsic loss versus group-velocity scaling behavior. In particular, Ref. 6 explicitly decomposed the loss into an out-of-plane scattering contribution and a backscattering contribution. Specifically, by calculating the *incoherent ensemble average* loss, where the loss predictions are representative of the results obtained when averaging the transmission spectra over many *nominally identical*, single-period experimental samples, the backscatter power loss per unit cell, α_{back}, and radiative loss, α_{rad}, were found to be[6]

$$\langle \alpha_{\text{back}}(\omega) \rangle = \frac{a^2 \omega^2}{4 v_g^2} \int \int \langle \Delta\varepsilon(\mathbf{r}) \Delta\varepsilon(\mathbf{r}') \rangle [\mathbf{e}_k(\mathbf{r}) \cdot \mathbf{e}_k(\mathbf{r})]$$
$$\times [\mathbf{e}_k^*(\mathbf{r}') \cdot \mathbf{e}_k^*(\mathbf{r}')] e^{2ik(x-x')} d\mathbf{r} d\mathbf{r}', \quad (1)$$

$$k = 0.34677 \times 2\pi/a$$

$$k = 0.3871 \times 2\pi/a$$

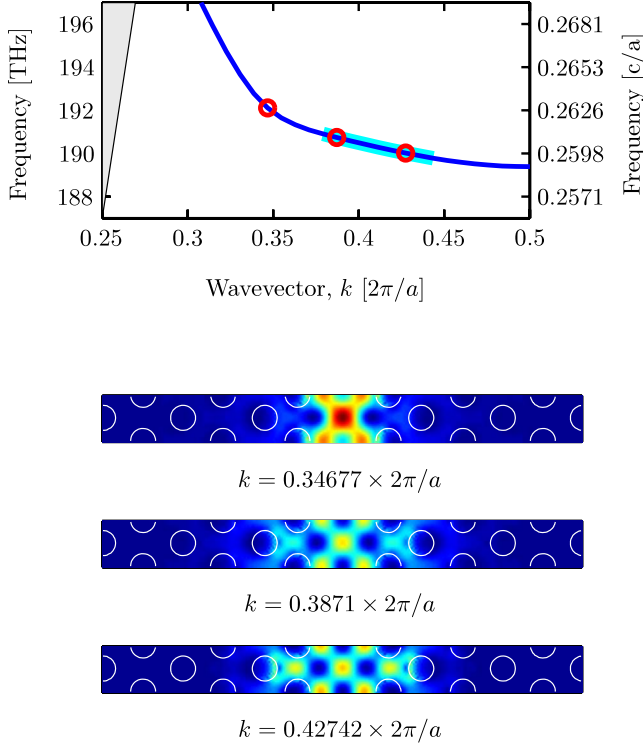$$k = 0.42742 \times 2\pi/a$$

FIG. 3. (Color online) Electric field distribution for various wave vectors in a dispersion engineered waveguide ($s_1 = -48$ nm, $s_2 = 16$ nm, $a = 410$ nm, and $r = 112$ nm, with a 220-nm-thick membrane). The top plot shows the dispersion relation in blue with the region of near-constant slow light highlighted in cyan. The three intensity plots show $|\mathbf{e}_k(\mathbf{r})|^2$ in the mid plane of the structure for each of the three wave vectors marked with red circles in the top plot.

$$\langle \alpha_{\mathrm{rad}}(\omega) \rangle = \frac{a\omega}{v_g} \int \int \langle \Delta\varepsilon(\mathbf{r})\Delta\varepsilon(\mathbf{r}') \rangle$$
$$\times \mathrm{Im}[\mathbf{e}_k^*(\mathbf{r}) \cdot \overleftrightarrow{\mathbf{G}}_{\mathrm{rad}}(\mathbf{r},\mathbf{r}',\omega) \cdot \mathbf{e}_k(\mathbf{r}') e^{ik(x'-x)}] d\mathbf{r}d\mathbf{r}',$$
$$(2)$$

where a is the pitch of the PC waveguide, $\mathbf{e}_k(\mathbf{r})$ is the ideal electric field Bloch mode with wave vector k and group velocity v_g, $\overleftrightarrow{\mathbf{G}}_{\mathrm{rad}}(\mathbf{r},\mathbf{r}',\omega)$ is an effective photon Green function for the radiation modes, and $\Delta\varepsilon(\mathbf{r})$ describes the difference between the ideal and disordered structure. The Green function is simply the electric field response at $\mathbf{r}$ to an oscillating polarization dipole at $\mathbf{r}'$. The electric fields are normalized by $\int_{\mathrm{unit\ cell}} \varepsilon_{\mathrm{ideal}}(\mathbf{r})[\mathbf{e}_k^*(\mathbf{r}) \cdot \mathbf{e}_k(\mathbf{r})] d\mathbf{r} = 1$. Similar to how we fit the dispersion data, we obtain the properties of the ideal waveguides with a plane-wave expansion technique.[24]

Consistent with other works, where good agreement has been found between theory and experiment,[5,12] we consider roughness on the surface of the holes to be the dominant source of scattering and so $\Delta\varepsilon(\mathbf{r})$ is nonzero only on the hole sidewall. A hole with a roughened surface is schematically illustrated in the inset of Fig. 1. The disorder correlation between two points on the sidewall of the same hole is taken to be: $\langle \Delta\varepsilon(\mathbf{r}_{\mathrm{side-wall}})\Delta\varepsilon(\mathbf{r}'_{\mathrm{side-wall}}) \rangle = (\varepsilon_2 - \varepsilon_1)^2 \sigma^2 e^{-r|\widetilde{\phi}-\widetilde{\phi}'|/l_p}$,
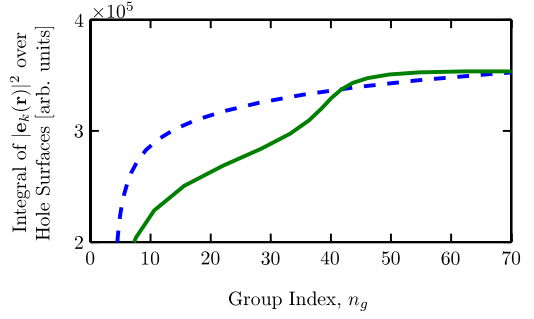

FIG. 4. (Color online) Integral of $|\mathbf{e}_k(\mathbf{r})|^2$ over the hole surfaces as a function of group index. The integral increases sharply at the designed group index due to restructuring of the electric field mode as shown in Fig. 3. The curves are for W1 waveguide (blue, dashed) and the dispersion engineered structure of Fig. 3 (green, solid). As can be recognized, this is most certainly *not* a constant.

where $\varepsilon_2 - \varepsilon_1$ is the change in dielectric constant, σ is the RMS roughness, r is the hole radius, $\widetilde{\phi} - \widetilde{\phi}'$ is the angle between the points measured from the hole center, and l_p is the correlation length measured around the circumference of the hole. Disorder between two points on different holes is taken to be uncorrelated, though this is not a model restriction. The roughness is taken to be perfectly correlated in the direction parallel to hole axis since it is assumed to be due to imperfections in the etching mask. This is similar to the statistical functions that have been fitted to images of photonic crystal slabs.[25] In this analysis, we have used disorder parameters of $\sigma = 2$ nm and $l_p = 40$ nm, which is consistent with our sample characterization and matches our experimental results.

Equations (1) and (2) predict an approximate group-velocity scaling of $1/v_g^2$ for backscattering and $1/v_g$ for out-of-plane scattering, however, the electric field Bloch mode, $\mathbf{e}_k(\mathbf{r})$, naturally changes simultaneously and thus its dependence on frequency cannot be neglected; this is a tempting analysis mistake in the expected scaling analysis for PC waveguides. The top plot of Fig. 3 shows the dispersion relation for a waveguide mode that has been engineered to have a region of low-dispersion slow light (highlighted in cyan). Three sample wave vectors are indicated with red circles and the associated Bloch mode electric field $|\mathbf{e}_k(\mathbf{r})|^2$ is shown in the bottom three plots. As the wave vector increases from 0.34677 to $0.3871 \times 2\pi/a$, the waveguide enters the slow-light region, and the electric field expands rapidly into the first row of the cladding PC where it interacts strongly with the disorder on the hole surfaces (this is similar to simple 2D PC calculations[26]). Importantly, the Bloch mode continues to change as the wave vector is further increased from 0.3871 to $0.42742 \times 2\pi/a$, despite the now constant group index.

To demonstrate this phenomenon more quantitatively, the integral of $|\mathbf{e}_k(\mathbf{r})|^2$ around the surfaces of the holes is shown in Fig. 4. This value captures the essence of the integral in Eq. (1) but is not directly proportional to the loss. In the figure, one can clearly see the sharp increase in the concentration of the electric field in the disorder region at the designed group index for the dispersion engineered structures

(green, solid). In contrast, the W1 waveguide (blue, dashed) has a mode distribution that evolves slowly with wave vector and does not exhibit this phenomenon. Whereas a simple $\alpha_{\text{back}} \propto v_g^{-2}$ relation (which is the standard assumption) would have predicted no change in loss with the group index held constant, the full calculation including the Bloch mode reveals a sharp increase in loss.

IV. BEYOND THE BEER-LAMBERT LAW

The above calculation technique yields the loss for a single period of a disordered waveguide. It is common to analyze waveguide transmission data assuming a Beer-Lambert dependence for the transmitted power $P(L)$, through a waveguide of length L: $P(L) = P_0 e^{-\alpha L}$. A Beer-Lambert relation is only appropriate for processes such as absorption where once light is lost from the forward propagating mode, it can never reach the output port. Although it is obvious that too much backscattering will cause the Beer-Lambert law to breakdown, hitherto, there are no convenient theoretical approaches to show this directly and thus no way of properly analyzing the experiments.

One resolution to the theory is to self-consistently model light propagation along an entire disordered waveguide, not just a single period.[12] Although this method provides a wealth of information, including sub unit-cell scattering and localization, it is computationally expensive and not suited for the common analysis of incoherent scattering losses. Instead, here we introduce a computationally simple calculation in Eqs. (1) and (2) to model a single period of the waveguide and then extrapolate the average loss per unit cell to long waveguides using an incoherently averaged coupled mode approach. With $\psi_f(x)$ and $\psi_b(x)$ giving the intensity in the forward and backward modes, respectively, the propagation is governed by (the frequency dependence is implicit)

$$\frac{d}{dx}\psi_f(x) = -(\alpha_{\text{back}} + \alpha_{\text{rad}})\psi_f(x) + \alpha_{\text{back}}\psi_b(x), \qquad (3)$$

$$\frac{d}{dx}\psi_b(x) = (\alpha_{\text{back}} + \alpha_{\text{rad}})\psi_b(x) - \alpha_{\text{back}}\psi_f(x), \qquad (4)$$

where α_{back} in the former (latter) case is associated with forward-back (back-forward) scattering. Using incoherent averages for the fully 3D loss coefficients [see Eqs. (1) and (2)], these equations are straightforward to solve analytically. With this technique, we do not expect to recover interesting coherent features such as Fabry-Pérot fringes and the variations in transmission on short frequency scales which are a phase effect as shown in Ref. 12. We do, however, reproduce the average transmission spectrum in a computationally efficient manner, which is more appropriate for analysis of experimental cut-back measurements.

By plotting the effective average loss per unit cell as a function of total waveguide length as done in Fig. 5 (solid) for four different frequencies, the failure of the Beer-Lambert law is undeniable. In the short waveguide limit, the effective loss coefficient is $\alpha_{\text{back}} + \alpha_{\text{rad}}$ (upper dashed limit). However in longer waveguides, the effective loss per unit cell *de-*
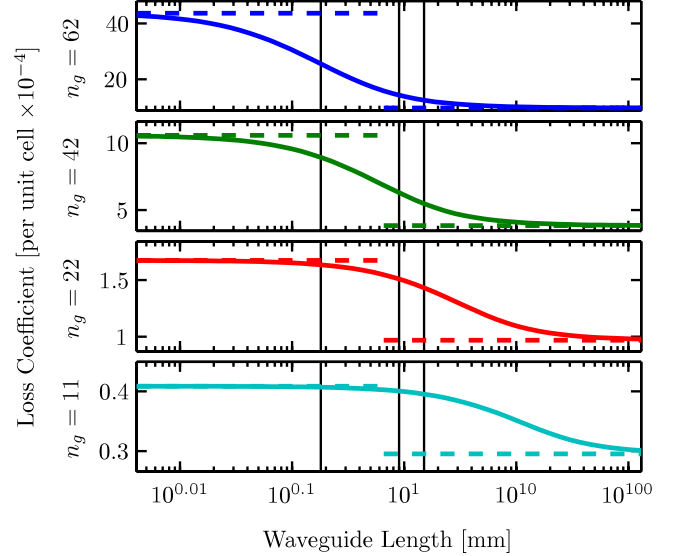

FIG. 5. (Color online) Average loss per unit cell (solid) as a function of waveguide length for the same structure as Fig. 6 at 190.4 THz, $n_g \simeq 62$ (top, blue); 191 THz, $n_g \simeq 42$ (second from top, green); 192 THz, $n_g \simeq 22$ (third from top, red); and 192.8 THz, $n_g \simeq 11$ (bottom, cyan); each plot here corresponds to a single frequency point on all three of the plots in Fig. 6. The three waveguide lengths of Fig. 6 are marked with vertical black lines. In the short waveguide limit, the loss coefficient is approximately $\alpha_{\text{back}} + \alpha_{\text{rad}}$ (upper dashed limit), in agreement with the Beer-Lambert results. In the long waveguide limit, the loss per unit cell decreases to $\sqrt{\alpha_{\text{rad}}^2 + 2\alpha_{\text{rad}}\alpha_{\text{back}}}$ (lower dashed limit) due to multiple scattering.

creases to $\alpha_{\text{rad}}\sqrt{1 + 2\alpha_{\text{back}}/\alpha_{\text{rad}}}$ (lower dashed limit) due to multiple scattering becoming significant. The multiple-scattering loss is strikingly different from the Beer-Lambert results (the upper dashed limit) and using it in the multiple-scattering regime will yield incorrect results. For example, the error in the loss per unit cell by a factor of 2 for the 1500 μm waveguide at $n_g \simeq 42$ is equivalent to an error in the total transmission by a factor of 6. In the fast light regime (e.g., $n_g \simeq 11$, bottom plot), backscattering is weak and the difference between short- and long-waveguide limits is minimal. This analysis is appropriate for c.w. excitation only; under pulsed excitation, multiple scattering will fragment the pulse and the meaning of a transmission amplitude is unclear.[12]

V. TRANSMISSION LOSSES: EXPERIMENTS AND THEORY

We have obtained a range of cut-back measurements for the samples discussed in Sec. II, and the data is shown in Fig. 6 by the blue curves. Superimposed are the calculated transmission spectra using a Beer-Lambert scaling relation (red, dashed) and using the incoherent multiple-scattering extrapolation (cyan, solid). In the fast light regime, the transmission is high and there is no significant difference between the Beer-Lambert and multiple-scattering predictions. However as the group velocity decreases and amplifies the scattering, the Beer-Lambert relation begins to overestimate the
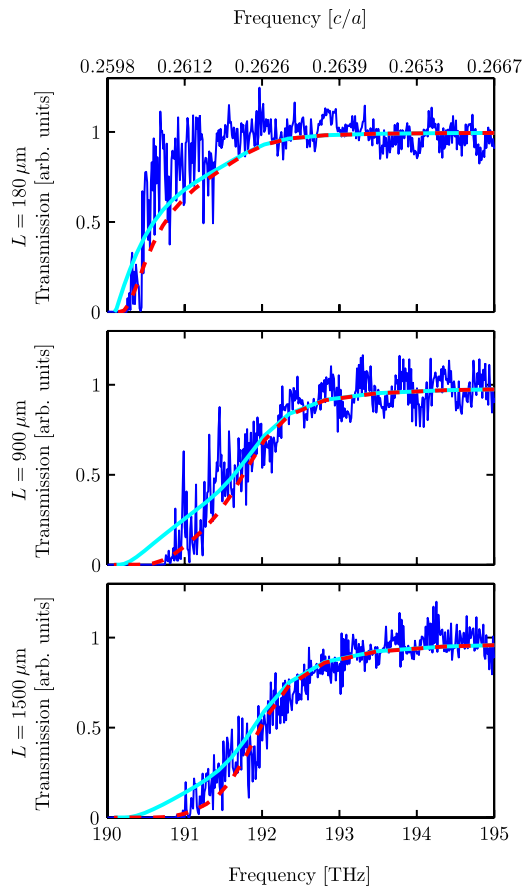
FIG. 6. (Color online) Comparison of empirical (blue) and calculated transmission spectra for $s_1 = -48$ nm and $s_2 = 16$ nm waveguides of various lengths. The calculated loss is shown extrapolated using the Beer-Lambert relation (red dashed) and the multiple-scattering method (cyan solid).

loss, even for the short 180 μm waveguide. The discrepancy becomes more pronounced for longer waveguides as multiple scattering become more probable. In particular, the Beer-Lambert relation predicts a steeper roll off than the multiple-scattering extrapolation and the experimental data. Very near the band edge, we underestimate the loss, most likely due to disorder-induced restructuring of the band structure[12,27,28] or disorder-induced modification of the mode cutoff[20] which we have not accounted for.

Due to the chosen sample parameters (especially the group index and the sample length), and because of inherent Fabry-Pérot noise in the measurements, these particular measurements are unable to clearly resolve the differences between the two theories. Although we have chosen a moderately slow waveguide, in principle, one could demonstrate this phenomenon more clearly by choosing waveguides with a plateau in the group index at a higher value (thereby increasing scattering). Nevertheless, Fig. 6 shows that the predictions between the two models are quantitatively different for realistic experimental samples and so multiple scattering should be included in the proper analysis of slow-light PC waveguides. Using the presented formalism, and carrying out a systematic investigation for various PC samples, one should certainly be able to show a more dramatic breakdown of the Beer-Lambert law.

VI. CONCLUSIONS

We have presented theoretical calculations and matching experiments for investigating the role of disorder-induced scattering in slow-light dispersion engineered structures. We have shown that, especially in dispersion engineered structures, the reshaping of the electric field Bloch mode is a significant contributor to the propagation loss. Further, interpreting transmission loss based on a Beer-Lambert relation fails in the slow-light regime where backscattering is enhanced, and multiple-scattering must be taken into account. We have presented a general technique to directly connect to the experiments in a straightforward way. Surprisingly, it is found that the Beer-Lambert law can break down for group indices as small as $n_g = 22$, showing that great care must be exercised if applying the Beer-Lambert law. These results highlight that the naïve view of simple group-velocity scaling for losses in PC waveguides in general does not apply, and that the fundamental Beer-Lambert law can break down dramatically in the multiple-scattering regime. For related effects of multiple-scattering in the coherent regime, see Ref. 12.

*shughes@physics.queensu.ca

†tfk@st-andrews.ac.uk

[1] M. Notomi, K. Yamada, A. Shinya, J. Takahashi, C. Takahashi, and I. Yokohama, Phys. Rev. Lett. **87**, 253902 (2001).

[2] Y. A. Vlasov, M. O'Boyle, H. F. Hamann, and S. J. McNab, Nature (London) **438**, 65 (2005).

[3] B. Corcoran, C. Monat, C. Grillet, D. J. Moss, B. J. Eggleton, T. P. White, L. O'Faolain, and T. F. Krauss, Nat. Photonics **3**, 206 (2009).

[4] T. Baba, Nat. Photonics **2**, 465 (2008).

[5] E. Kuramochi, M. Notomi, S. Hughes, A. Shinya, T. Watanabe, and L. Ramunno, Phys. Rev. B **72**, 161318(R) (2005).

[6] S. Hughes, L. Ramunno, J. F. Young, and J. E. Sipe, Phys. Rev. Lett. **94**, 033903 (2005).

[7] D. Gerace and L. C. Andreani, Opt. Lett. **29**, 1897 (2004).

[8] M. L. Povinelli, S. G. Johnson, E. Lidorikis, J. D. Joannopoulos, and M. Soljacic, Appl. Phys. Lett. **84**, 3639 (2004).

[9] S. John, Phys. Rev. Lett. **53**, 2169 (1984).

[10] P. W. Anderson, Philos. Mag. B **52**, 505 (1985).

[11] D. S. Wiersma and A. Lagendijk, Phys. Rev. E **54**, 4256 (1996).

[12] M. Patterson, S. Hughes, S. Combrié, N.-V.-Quynh Tran, A. De Rossi, R. Gabet, and Y. Jaouën, Phys. Rev. Lett. **102**, 253903 (2009).

[13] B. Wang, S. Mazoyer, J. P. Hugonin, and P. Lalanne, Phys. Rev. B **78**, 245108 (2008).

[14] R. J. P. Engelen, D. Mori, T. Baba, and L. Kuipers, Phys. Rev. Lett. **101**, 103901 (2008).

[15] L. H. Frandsen, A. V. Lavrinenko, J. Fage-Pedersen, and P. I. Borel, Opt. Express **14**, 9444 (2006).

[16] S. Kubo, D. Mori, and T. Baba, Opt. Lett. **32**, 2981 (2007).

[17] J. Li, T. P. White, L. O'Faolain, A. Gomez-Iglesias, and T. F. Krauss, Opt. Express **16**, 6227 (2008).

[18] Y. Hamachi, S. Kubo, and T. Baba, Opt. Lett. **34**, 1072 (2009).

[19] A. Y. Petrov and M. Eich, Appl. Phys. Lett. **85**, 4866 (2004).

[20] L. O'Faolain, T. P. White, D. O'Brien, X. Yuan, M. D. Settle, and T. F. Krauss, Opt. Express **15**, 13129 (2007).

[21] J. P. Hugonin, P. Lalanne, T. P. White, and T. F. Krauss, Opt. Lett. **32**, 2638 (2007).

[22] D. M. Beggs, L. O'Faolain, and T. F. Krauss, Photonics Nanostruct. Fundam. Appl. **6**, 213 (2008).

[23] A. Gomez-Iglesias, D. O'Brien, L. O'Faolain, A. Miller, and T. F. Krauss, Appl. Phys. Lett. **90**, 261107 (2007).

[24] S. G. Johnson and J. D. Joannopoulos, Opt. Express **8**, 173 (2001).

[25] M. Skorobogatiy, G. Bégin, and A. Talneau, Opt. Express **13**, 2487 (2005).

[26] A. Petrov, M. Krause, and M. Eich, Opt. Express **17**, 8676 (2009).

[27] J. G. Pedersen, S. Xiao, and N. A. Mortensen, Phys. Rev. B **78**, 153101 (2008).

[28] D. P. Fussell, S. Hughes, and M. M. Dignam, Phys. Rev. B **78**, 144201 (2008).